

Matched asymptotic solutions for the steady banded flow of the diffusive Johnson-Segalman model in various geometries^{*}

O. Radulescu¹ and P. D. Olmsted²

Department of Physics and Astronomy, and IRC in Polymer Science and Technology, University of Leeds, Leeds LS2 9JT, United Kingdom

Abstract

We present analytic solutions for steady flow of the Johnson-Segalman (JS) model with a diffusion term in various geometries and under controlled strain rate conditions, using matched asymptotic expansions. The diffusion term represents a singular perturbation that lifts the continuous degeneracy of stable, banded, steady states present in the absence of diffusion. We show that the stable steady flow solutions in Poiseuille and cylindrical Couette geometries always have two bands. For Couette flow and small curvature, two different banded solutions are possible, differing by the spatial sequence of the two bands.

1 Introduction

Many experimental results confirm the possibility of shear banding, i.e. the separation of bands of different shear rates and apparent viscosities in the flow of various systems of wormlike micelles (aqueous solutions of surfactants and salt [1–5] or organic solvent solutions of metallic complexes [6]), or lyotropic liquid crystals [7]. This type of behaviour can be explained as being the result of a constitutive instability, suitably described by non-monotonic flow curves such as those arising from the Johnson-Segalman (JS) [8] or Doi-Edwards models [9]. It is possible that similar constitutive instabilities are responsible for spurt and extrudate distortions of polymer melts [10].

^{*} Submitted to *Journal of Non-Newtonian Fluid Mechanics*

¹ phyor@irc@leeds.ac.uk

² p.d.olmsted@leeds.ac.uk

The steady banded flow solutions of the JS model were previously studied in planar [11,12], Poiseuille [13–17], and cylindrical Couette geometries [18]. In all these geometries banded flow solutions have continuous degeneracy [16,17,19], resulting from the indeterminacy of the positions of the interfaces and of the number of bands. The stress value can be kinetically selected [20,12,18,16,17], and it may differ from the top jump prediction of Refs. [13,14], although the selected value depends on the flow history and on the imposed shear rate [19]. This is in contrast to experiments on wormlike micelles that show a well defined stress plateau in the flow curves: the total stress is history independent and do not change with the shear rate. Furthermore, the evolution of the stress during transient flow may be rather long, suggesting the slow migration of the interface between bands to an equilibrium position [2].

Recently [19,21,22] we showed that, by supplementing the JS model with a stress diffusion term, one can lift the degeneracy of the steady flow and also account for the slow migration of the interface. The origin of this diffusion term can be justified in terms of the Brownian movement of polymer chains in an inhomogeneous stress field and can be deduced from the Fokker-Planck equation for a system of dumbbells [23]. There is no calculation, at present, for such a term in the wormlike micelle system. Similar results have been obtained by Refs. [24,25] by introducing phenomenological diffusion terms in toy constitutive models. Although non-local terms are not important in homogeneous flow, in banded flow a realistic description of interfaces as strongly inhomogeneous regions requires such terms. This necessity has been noted by many authors [23,26–28].

Recent experiments [29] on wormlike micelles in pipe (Poiseuille) and cylindrical Couette flow geometries, or in cone and plate [30] using NMR microscopy found shear rate profiles with two or three bands. Birefringence measurements in Couette geometry [31,32] suggest the existence of only two bands, although the relation between birefringence and shear rate is hard to establish because it depends on microstructure. Most experiments on shear banding are performed in geometries imposing inhomogeneous total stress (Couette, pipe flow, cone and plate). Typically a stress quantity (*e.g.* torque, or pressure drop, or shear stress) is measured as a function of a rate of flow quantity (*e.g.* mean strain rate, flux through a pipe, wall speed), and an engineering “flow curve” is constructed. Under inhomogeneous flow conditions the flow curves are not simply the local constitutive relation of the fluid. It is therefore important to assess theoretically the question of how many bands can occur and which are the flow curves for a given constitutive model and in various geometries.

We present elsewhere numerical computations of flow curves in Couette flow [19] for the JS-d model. Here we show how matched asymptotics techniques can be used to obtain analytic results on the number of bands, interface width, and flow curves in various geometries. The application of these techniques to

the JS-d model represents only an example, and the same method can be easily adapted to other constitutive models.

The structure of the paper is the following. In Section 2 we introduce the flow equations in various geometries. The matched asymptotic solutions of these equations are presented in Section 3. In Section 4 we discuss how the inner layer solution controls the history independence and stability of the flow. We apply our results in Section 5 to predict the shapes of flow curves and the interface width. In Section 6 we discuss the results and suggest possible extensions.

2 Flow equations in various geometries

2.1 General equations

The dynamics of the diffusive Johnson-Segalman fluid is described by two equations. The first is the momentum balance:

$$\rho (\partial_t + \mathbf{v} \cdot \nabla) \mathbf{v} = \nabla \cdot \mathbf{T}, \quad (2.1)$$

where ρ is the fluid density, \mathbf{v} is the velocity field, and $\mathbf{T} = -p \mathbf{I} + 2\eta \mathbf{D} + \Sigma$ is the total stress tensor where the pressure p is determined by incompressibility, Σ is the viscoelastic stress carried by the polymer strands, η is the “solvent viscosity” and \mathbf{D} is the symmetric part of the velocity gradient. The second equation is a constitutive relation for the polymer stress Σ , which we take to be the the JS constitutive model [8] with an added diffusion term [21,19]:

$$\overset{\blacklozenge}{\Sigma} = \mathcal{D} \nabla^2 \Sigma + 2 \frac{\mu}{\tau} \mathbf{D} - \frac{1}{\tau} \Sigma, \quad (2.2)$$

where μ is the “polymer” viscosity, τ is the relaxation time, and \mathcal{D} is the diffusion coefficient.

The time evolution of Σ is governed by the Gordon-Schowalter (GS) time derivative [33],

$$\overset{\blacklozenge}{\Sigma} = (\partial_t + \mathbf{v} \cdot \nabla) \Sigma - (\mathbf{\Omega} \Sigma - \Sigma \mathbf{\Omega}) - a (\mathbf{D} \Sigma + \Sigma \mathbf{D}) \quad (2.3)$$

where a is the “slip parameter” and $\mathbf{\Omega}$ is the antisymmetric part of the velocity gradient. For $a = 1$ there is no slip and the GS derivative becomes the upper convective derivative. For $a = 0$ (total slip) the fluid stress is not transmitted to the polymer strands and these can only be oriented by the flow: the GS derivative becomes the corotational derivative. In this work we consider $|a| < 1$.

We study the case of a fixed average shear rate, which represents a global constraint on the velocity gradient. We discuss several shear geometries: planar shear, slit and pipe Poiseuille flow, and cylindrical Couette flow between concentric cylinders. We consider parallel stream lines in all geometries and leave the possibility of secondary flow for further investigation.

2.2 Planar shear and Poiseuille flow

Parallel stream line flow corresponds to $\mathbf{v} = v(y)\mathbf{e}_x$, for planar shear between plates at positions $y = 0, L$ and for Poiseuille flow through a rectangular slit of infinite length and walls at positions $y = \pm L$.

We introduce dimensionless variables, $\hat{V} = -V\frac{\tau}{L}\sqrt{1-a^2}\hat{W} = (\frac{1-a}{2}\Sigma_{yy} - \frac{1+a}{2}\Sigma_{xx})\frac{\tau}{\mu}$, $\hat{\gamma} = \dot{\gamma}\tau\sqrt{1-a^2}$, $\hat{Z} = (\frac{1-a}{2}\Sigma_{yy} + \frac{1+a}{2}\Sigma_{xx})\frac{\tau}{\mu}$, $\hat{S} = \Sigma_{yx}\frac{\tau}{\mu}\sqrt{1-a^2}$, $\hat{D} = \mathcal{D}\frac{\tau}{L^2}$, $f = \frac{\partial p}{\partial x}\frac{L\sqrt{1-a^2}}{\mu\tau}$, $\hat{\sigma} = T_{yx}\frac{\tau}{\mu}\sqrt{1-a^2}$, $\hat{t} = t/\tau$, $\hat{r} = y/L$. V is the velocity at $y = 0$ (the maximum absolute value), having opposite sign to the shear rate and stress. With these definitions \hat{V} has the same sign as the reduced shear rate and stress. In terms of these quantities the momentum balance reads:

$$\alpha\partial_{\hat{t}}\hat{V} = \partial_{\hat{r}}\hat{S} + \epsilon\partial_{\hat{r}}^2\hat{V} - f. \quad (2.4)$$

The dimensionless pressure gradient f vanishes in planar shear, $\epsilon = \frac{\eta}{\mu}$ is the retardation parameter (viscosity ratio) and $\alpha = \frac{\rho L^2}{\mu\tau}$ is the ratio of the Reynolds and the Weissenberg numbers. In shear-banding experiments (*e.g.* for wormlike micelles) $\alpha \sim 10^{-4} - 10^{-3}$, therefore in this case one can neglect inertia and replace Eq. (2.4) by its creeping flow limit:

$$\partial_{\hat{r}}(\epsilon\hat{\gamma} + \hat{S}) = 0 \quad (2.5)$$

The solutions of Eq. (2.5) are:

$$\hat{\sigma}(\hat{r}) = \text{const} \quad (\text{planar shear}) \quad (2.6a)$$

$$\hat{\sigma}(\hat{r}) = f\hat{r} \quad (\text{slit Poiseuille}). \quad (2.6b)$$

where $\hat{\sigma} := \epsilon\hat{\gamma} + \hat{S}$ is the total stress.

The constitutive equations read

$$\partial_{\hat{t}}\hat{S} = \hat{D}\partial_{\hat{r}}^2\hat{S} - \hat{S} + \hat{\gamma}(1 - \hat{W}) \quad (2.7a)$$

$$\partial_{\hat{t}}\hat{W} = \hat{D}\partial_{\hat{r}}^2\hat{W} - \hat{W} + \hat{\gamma}\hat{S} \quad (2.7b)$$

$$\partial_{\hat{t}}\hat{Z} = \hat{D}\partial_{\hat{r}}^2\hat{Z} - \hat{Z}, \quad (2.7c)$$

and the shear rate condition is:

$$\hat{V} = \int_0^1 \hat{\gamma}(\hat{r}) d\hat{r}. \quad (2.8)$$

2.3 Cylindrical Couette flow

In the Couette geometry with concentric cylinders at radii $R_1 < R_2$ and assuming circular stream lines we have $\mathbf{v} = v(r)\mathbf{e}_\theta$. The momentum balance in cylindrical coordinates reads $\alpha \partial_t \hat{v} = \frac{1}{\hat{r}^2} \partial_{\hat{r}} [\hat{r}^2 (\hat{S} + \epsilon \hat{\gamma})]$, where $\hat{\gamma} = \hat{r} \frac{\partial}{\partial \hat{r}} \left(\frac{\hat{v}}{\hat{r}} \right)$ is the shear rate and $\alpha = \frac{\rho R_1^2}{\mu \tau}$ has the same significance as in planar shear. Creeping flow corresponds to:

$$\epsilon \hat{\gamma} + \hat{S} = \hat{\sigma}(\hat{r}) = \frac{\hat{\Gamma}}{\hat{r}^2}. \quad (2.9)$$

The constitutive equations read

$$\partial_t \hat{S} = \hat{D} \Delta_{\hat{r}} \hat{S} - \hat{S} \left[1 + \frac{4\hat{D}}{(1-a^2)\hat{r}^2} \right] + \hat{\gamma}(1 - \hat{W}) \quad (2.10a)$$

$$\partial_t \hat{W} = \hat{D} \Delta_{\hat{r}} \hat{W} - \hat{W} + \left[\hat{\gamma} - \frac{4\hat{D}}{(1-a^2)\hat{r}^2} \right] \hat{S} \quad (2.10b)$$

$$\partial_t \hat{Z} = \hat{D} \Delta_{\hat{r}} \hat{Z} - \hat{Z} \left[1 - \frac{4\hat{D}a^2}{(1-a^2)\hat{r}^2} \right] + \frac{4\hat{D}a}{(1-a^2)\hat{r}^2} \hat{W} \quad (2.10c)$$

where $\Delta_{\hat{r}} = \partial_{\hat{r}}^2 + \frac{1}{\hat{r}} \partial_{\hat{r}}$ is the Laplacian. The shear rate condition is:

$$\hat{V} = \int_1^{1+p} \hat{\gamma}(\hat{r}) \frac{d\hat{r}}{\hat{r}} \quad (2.11)$$

where $p = \frac{R_2 - R_1}{R_1}$.

All the above variables are dimensionless and have the same sign, with the following definitions: $\hat{V} = -V \frac{\tau}{R_1} \sqrt{1-a^2}$, $\hat{W} = \left(\frac{1-a}{2} \Sigma_{\theta\theta} - \frac{1+a}{2} \Sigma_{rr} \right) \frac{\tau}{\mu}$, $\hat{Z} = \left(\frac{1-a}{2} \Sigma_{\theta\theta} + \frac{1+a}{2} \Sigma_{rr} \right) \frac{\tau}{\mu}$, $\hat{S} = \Sigma_{r\theta} \frac{\tau}{\mu} \sqrt{1-a^2}$, $\hat{D} = \mathcal{D} \frac{\tau}{R_1^2}$, $\hat{\Gamma} = -\Gamma \frac{\tau \sqrt{1-a^2}}{\mu R_1^2}$, $\hat{\sigma} = T_{r\theta} \frac{\tau}{\mu} \sqrt{1-a^2}$, and $\hat{r} = r/R_1$. Γ is the torque per unit length applied at the inner cylinder, and has the same sign as V , the velocity of the inner cylinder, being opposite to the shear rate and stress. With these definitions $\hat{\Gamma}$ and \hat{V} have the same sign as the shear rate and stress.

2.4 Pipe flow

Like for Couette flow we use cylindrical coordinates, with the z axis parallel to the stream lines, $\mathbf{v} = v(r)\mathbf{e}_z$. The pipe is an infinite length cylinder of radius R . The momentum balance reads $\alpha\partial_t\hat{v} = \frac{1}{\hat{r}}\partial_{\hat{r}}[\hat{r}(\hat{S} + \epsilon\hat{\gamma})] - 2f$, where $\hat{\gamma} = \frac{\partial\hat{v}}{\partial\hat{r}}$ is the shear rate. Creeping flow corresponds to a total stress that is linear in \hat{r} , like for the slit geometry:

$$\epsilon\hat{\gamma} + \hat{S} = \hat{\sigma}(\hat{r}) = f\hat{r}. \quad (2.12)$$

The shear rate condition is:

$$\hat{V} = \int_0^1 \hat{\gamma}(\hat{r})d\hat{r}. \quad (2.13)$$

The constitutive equations are:

$$\partial_t\hat{S} = \hat{D}\Delta_{\hat{r}}\hat{S} - \hat{S}\left[1 + \frac{\hat{D}}{\hat{r}^2}\right] + \hat{\gamma}(1 - \hat{W}) \quad (2.14a)$$

$$\partial_t\hat{W} = \hat{D}\Delta_{\hat{r}}\hat{W} - \hat{W} + \hat{\gamma}\hat{S} - \frac{4\hat{D}\hat{X}}{\hat{r}^2} \quad (2.14b)$$

$$\partial_t\hat{Z} = \hat{D}\Delta_{\hat{r}}\hat{Z} - \hat{Z} + \frac{\hat{D}\hat{X}}{\hat{r}^2} \quad (2.14c)$$

$$\partial_t\hat{X} = \hat{D}\Delta_{\hat{r}}\hat{X} + \hat{X}\left[1 + \frac{4\hat{D}}{\hat{r}^2}\right] - \hat{\gamma}\hat{S} \quad (2.14d)$$

We have used the following rescalings: $\hat{V} = -V_z\frac{\tau}{R}\sqrt{1-a^2}$, $\hat{W} = (\frac{1-a}{2}\Sigma_{zz} - \frac{1+a}{2}\Sigma_{rr})\frac{\tau}{\mu}$, $\hat{X} = (\Sigma_{\theta\theta} - \Sigma_{zz})\frac{\tau(1+a)}{\mu}$, $\hat{Z} = (\frac{1-a}{2}\Sigma_{zz} + \frac{1+a}{2}\Sigma_{rr})\frac{\tau}{\mu}$, $\hat{S} = \Sigma_{rz}\frac{\tau}{\mu}\sqrt{1-a^2}$, $f = \frac{1}{2}\frac{\partial p}{\partial z}\frac{R\sqrt{1-a^2}}{\mu\tau}$, $\hat{D} = \mathcal{D}\frac{\tau}{R^2}$, and $\hat{r} = r/R$.

3 Matched asymptotic solution for the steady flow

The flow is described by the system of nonlinear, parabolic partial differential equations of the reaction-diffusion type, Eqs. (2.7), (2.10), or (2.14). The nonlinear reaction terms are due to the polymer stress relaxation. The non-affine deformation (slip) is essential for the nonlinearity, and all rescalings are possible for $|a| < 1$.

We consider small \hat{D} , for which the diffusion terms represent a small perturbation to the steady flow equations. Nevertheless, this perturbation is singular and the solution can not be represented as a uniformly convergent power series in \hat{D} . The usual technique applying to this situation is asymptotic matching

[34]. The solution is divided into an inner layer solution around the interface where the diffusion terms are important and outer layer solutions a distance from the interface farther than its width (that scales like $\hat{D}^{1/2}$), where diffusion terms are exponentially small and can be neglected.

3.1 Outer layer solution

Neglecting terms of order \hat{D} and imposing stationarity in any of either Eqs. (2.6) and (2.7), or Eqs. (2.9) and (2.10), or Eqs. (2.12) and (2.14), depending on geometry, we obtain the same equations:

$$\hat{\gamma}_{out} = \frac{\hat{\sigma}(\hat{r}) - \hat{S}_{out}}{\epsilon} \quad (3.1a)$$

$$\hat{S}_{out} = \frac{\hat{\sigma}(\hat{r}) - \hat{S}_{out}}{\epsilon} (1 - \hat{W}_{out}) \quad (3.1b)$$

$$\hat{W}_{out} = \hat{S}_{out} \frac{\hat{\sigma}(\hat{r}) - \hat{S}_{out}}{\epsilon} \quad (3.1c)$$

$$\hat{Z}_{out} = 0. \quad (3.1d)$$

For pipe flow we may also use $\hat{X}_{out} = \hat{W}_{out}$ that together with Eq. (3.1d) implies $(\Sigma_{\theta,\theta})_{out} = 0$.

The algebraic system of Eqs. (3.1) is parametrised by $\hat{\sigma}$, the value of the total stress at the position \hat{r} in the gap. The shear rate $\hat{\gamma}$, as a function of the total stress $\hat{\sigma}$ represents the local constitutive curve shown in Fig. 1a. Banded flow is possible between the minimum ($\hat{\sigma} = \sigma_{bottom}(\epsilon)$) and the maximum ($\hat{\sigma} = \sigma_{top}(\epsilon)$) of the flow curve, when for one value of the stress there are three possible solutions of Eqs. (3.1). Only two of those (low $\{\hat{\gamma}^-(\hat{\sigma}), \hat{S}^-(\hat{\sigma}), \hat{Z}^-(\hat{\sigma})\}$ and high shear rate $\{\hat{\gamma}^+(\hat{\sigma}), \hat{S}^+(\hat{\sigma}), \hat{Z}^+(\hat{\sigma})\}$) correspond to stable bands, the intermediate shear rate being unstable [13,14]. The dependence of σ_{bottom} and σ_{top} on ϵ can be obtained from Eqs. (3.1), and is represented in Fig. 1b.

3.2 Inner layer solution

In any of the Eqs. (2.6) and (2.7), or Eqs. (2.9) and (2.10), or Eqs. (2.12) and (2.14), we impose stationarity and change variables to:

$$\tilde{r} = \frac{\hat{r} - \hat{r}^*}{\sqrt{\hat{D}}} \quad (3.2)$$

where \hat{r}^* is the position of the interface.

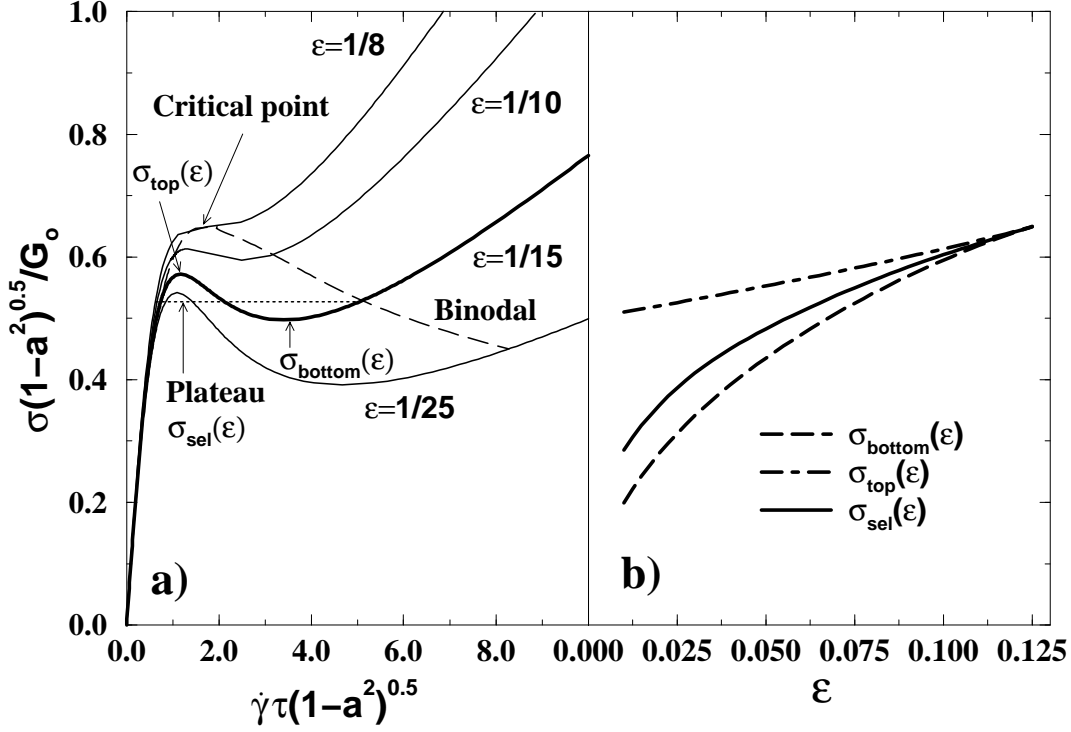


Fig. 1. a) Local constitutive curves in reduced variables, for different retardation parameters ϵ , analogous to the van der Waals liquid-gas isotherms. The extremities of the stress plateau, for different ϵ , form the binodal curve. Above $\epsilon = 1/8$ (critical point) the constitutive curve is monotonic. The homogeneous branches and the plateau constitute the flow curve in planar shear. b) Limiting values of the stress allowing coexistence of bands, as functions of the retardation parameter ϵ . σ_{sel} is the selected stress value at the interface. The values are consistent with the results in [21] obtained with a different method.

The stress is expanded about the interface position, $\hat{\sigma} = \hat{\sigma}^* + \hat{D}^{1/2}\tilde{r}\partial_{\tilde{r}}\hat{\sigma} + \mathcal{O}(\hat{D})$, where $\hat{\sigma}^* = \hat{\sigma}(\hat{r}^*)$ is the value of the stress at the interface. By neglecting terms of order $\hat{D}^{1/2}$ and higher we obtain, for all studied geometries:

$$\partial_{\tilde{r}}^2 \hat{S}_{in} = \hat{S}_{in} - \frac{\hat{\sigma}^* - \hat{S}_{in}}{\epsilon} (1 - \hat{W}_{in}) \quad (3.3a)$$

$$\partial_{\tilde{r}}^2 \hat{W}_{in} = \hat{W}_{in} - \frac{\hat{S}_{in}(\hat{\sigma}^* - \hat{S}_{in})}{\epsilon} \quad (3.3b)$$

$$\hat{Z}_{in} = 0 \quad (3.3c)$$

For pipe flow we may also use $\hat{X}_{in} = \hat{W}_{in}$, that together with Eq. (3.3c) implies $(\Sigma_{\theta,\theta})_{in} = 0$.

We refer here only to single interface solutions. More complex solutions with an arbitrary number of interfaces can be treated in the same way. There are two types of single interface solutions, differing by the sequence of bands. Let

us refer to the solution with the high shear rate band at the left of the interface (towards smaller \hat{r}) as $(+-)$, and to the solution with the high shear rate band at the right of the interface (towards bigger \hat{r}) as $(-+)$.

The inner and outer solutions should match at the interface (Prandtl matching principle, Ref. [34]), leading for the sequence $(+-)$ to:

$$\hat{S}_{in}^{+-}(-\infty) = \hat{S}_{out}^+(\hat{\sigma}^*) \quad \hat{W}_{in}^{+-}(-\infty) = \hat{W}_{out}^+(\hat{\sigma}^*) \quad (3.4a)$$

$$\hat{S}_{in}^{+-}(\infty) = \hat{S}_{out}^-(\hat{\sigma}^*) \quad \hat{W}_{in}^{+-}(\infty) = \hat{W}_{out}^-(\hat{\sigma}^*) \quad (3.4b)$$

or for the sequence $(-+)$ to:

$$\hat{S}_{in}^{-+}(-\infty) = \hat{S}_{out}^-(\hat{\sigma}^*) \quad \hat{W}_{in}^{-+}(-\infty) = \hat{W}_{out}^-(\hat{\sigma}^*) \quad (3.4c)$$

$$\hat{S}_{in}^{-+}(\infty) = \hat{S}_{out}^+(\hat{\sigma}^*). \quad \hat{W}_{in}^{-+}(\infty) = \hat{W}_{out}^+(\hat{\sigma}^*) \quad (3.4d)$$

3.3 Equations of flow curves

The flow curve expresses the relation between measurable quantities: velocity of the inner cylinder \hat{V} and torque $\hat{\Gamma}$ in the Couette geometry, maximum velocity \hat{V} and pressure gradient f in Poiseuille flow, gap velocity \hat{V} and shear stress $\hat{\sigma}$ in planar shear.

In order to obtain the flow curves we use the shear rate conditions, Eqs. (2.8), (2.11), (2.13), and the relations (2.6b), (2.9), (2.12) between the total stress $\hat{\sigma}$ and the position \hat{r} . In the banded regime, the shape of the flow curve depends on the number of interfaces and on the sequence of bands. We shall show in the next section that in the presence of stress diffusion steady flow always corresponds or can be reduced by symmetry to a single interface.

In Poiseuille flow, using Eqs. (2.6b), (2.8) or (2.12), (2.13), a single interface flow curve with the high shear rate band near the wall (right of the interface) is described by:

$$\hat{V}(f, \hat{\sigma}^*) = \frac{1}{f} \left[\int_0^{\hat{\sigma}^*} \hat{\gamma}^-(\hat{\sigma}) d\hat{\sigma} + \int_{\hat{\sigma}^*}^f \hat{\gamma}^+(\hat{\sigma}) d\hat{\sigma} \right] \quad (3.5)$$

where $\hat{\sigma}^* = \hat{\sigma}(\hat{r}^*)$ is the value of the total stress at the position of the interface. The inverse sequence of bands is prohibited in Poiseuille flow, because the high shear rate band can not exist at $\hat{r} = 0$, where $\hat{\sigma} = 0$.

In Couette flow, using Eqs. (2.9), (2.11) a single interface flow curve with the

high shear rate band near the inner cylinder (left of the interface) is given by:

$$\hat{V}^{+-}(\hat{\Gamma}, \hat{\sigma}^*) = \frac{1}{2} \left[\int_{\hat{\Gamma}/(1+p)^2}^{\hat{\sigma}^*} \hat{\gamma}^-(\hat{\sigma}) \frac{d\hat{\sigma}}{\hat{\sigma}} + \int_{\hat{\sigma}^*}^{\hat{\Gamma}} \hat{\gamma}^+(\hat{\sigma}) \frac{d\hat{\sigma}}{\hat{\sigma}} \right] \quad (3.6)$$

The flow curve for the inverse sequence of bands (high shear rate band near the outer cylinder) is given by:

$$\hat{V}^{-+}(\hat{\Gamma}, \hat{\sigma}^*) = \frac{1}{2} \left[\int_{\hat{\Gamma}/(1+p)^2}^{\hat{\sigma}^*} \hat{\gamma}^+(\hat{\sigma}) \frac{d\hat{\sigma}}{\hat{\sigma}} + \int_{\hat{\sigma}^*}^{\hat{\Gamma}} \hat{\gamma}^-(\hat{\sigma}) \frac{d\hat{\sigma}}{\hat{\sigma}} \right] \quad (3.7)$$

Planar flow represents a special case because the total stress is constant throughout the gap (Eq. (2.6a)) and thus:

$$\hat{V}(\nu, \hat{\sigma}) = \nu \hat{\gamma}^+(\hat{\sigma}) + (1 - \nu) \hat{\gamma}^-(\hat{\sigma}) \quad (3.8)$$

where ν is the proportion of high shear rate band in the flow. As we shall argue below, the flow curves above are well defined because the value $\hat{\sigma}^*$ of the shear stress at the interface is a geometry-independent constant.

4 Uniqueness and stability of the steady flow

4.1 An existence conjecture for the inner layer solution

The inner layer solution controls the existence and stability of steady banded flows. Because we are dealing with singular perturbations, this control can be performed even by a very thin interface (very small \hat{D}). Before stating an important property of the inner layer solution, we note that steady banded flow is a particular case of a moving interface solution $\hat{r}^*(t)$. We may look for matched asymptotic solutions in this case as well and one may show by using the change of variable

$$\tilde{r} = \frac{\hat{r} - \hat{r}^*(t)}{\sqrt{\hat{D}}} \quad (4.1)$$

that the moving interface inner layer solution should obey:

$$\partial_{\tilde{r}}^2 \hat{S}_{in} + c \partial_{\tilde{r}} \hat{S}_{in} = \hat{S}_{in} - \frac{\hat{\sigma}^* - \hat{S}_{in}}{\epsilon} (1 - \hat{W}_{in}) \quad (4.2a)$$

$$\partial_{\tilde{r}}^2 \hat{W}_{in} + c \partial_{\tilde{r}} \hat{W}_{in} = \hat{W}_{in} - \frac{\hat{S}_{in}(\hat{\sigma}^* - \hat{S}_{in})}{\epsilon} \quad (4.2b)$$

where

$$c = \frac{1}{\sqrt{\hat{D}}} \frac{d\hat{r}^*(t)}{dt} \quad (4.3)$$

is the rescaled velocity of the interface.

Conjecture. *There is a unique value $\hat{\sigma}^* = \hat{\sigma}_{sel} \in (\sigma_{bottom}(\epsilon), \sigma_{top}(\epsilon))$ of the total shear stress at the position of the interface, such that a steady inner layer solution for the banded flow of the JS-d model (Eqs. (3.3)) exists obeying the Prandtl matching principle, Eqs. (3.4). Moreover, moving interface inner layer solutions obeying the Prandtl matching principle for Eqs. (4.2) exist for values of $\hat{\sigma}^*$ in a neighbourhood of $\hat{\sigma}_{sel}$, with velocities $c(\hat{\sigma}^*)$ that are well defined functions of $\hat{\sigma}^*$. The stationary solution satisfies $c(\hat{\sigma}_{sel}) = 0$ and, furthermore, $\frac{dc}{d\hat{\sigma}^*}|_{\hat{\sigma}_{sel}} > 0$ when the high shear rate band is at the left (towards smaller values of \hat{r}) of the interface, and $\frac{dc}{d\hat{\sigma}^*}|_{\hat{\sigma}_{sel}} < 0$ for the inverse sequence of bands.*

Remark 1. The conjecture considers the inner layer solution, which obeys the same equation for all flow geometries. This implies that the selected value of the stress is geometry-independent. After the rescalings, the diffusion coefficient does not enter Eqs. (4.2). Thus, the selected stress is independent of \mathcal{D} . As shown by Eq. (4.3) the speed of the interface $d\hat{r}^*/dt$ scales with $\hat{D}^{1/2}$, thus the rôle of \hat{D} is to speed up kinetics of non-steady flow.

Remark 2. A stationary inner layer solution which obeys the Prandtl matching principle represents a heteroclinic orbit of the 4D dynamical system $\{\hat{S}, \partial_{\hat{r}}\hat{S}, \hat{W}, \partial_{\hat{r}}\hat{W}\}$, connecting the hyperbolic fixed points $\{\hat{S}^+(\hat{\sigma}_{sel}), 0, \hat{W}^+(\hat{\sigma}_{sel}), 0\}$ and $\{\hat{S}^-(\hat{\sigma}_{sel}), 0, \hat{W}^-(\hat{\sigma}_{sel}), 0\}$. As discussed in [19,21], and as is valid rather generally in these cases, the value of the parameter $\hat{\sigma}^* = \hat{\sigma}_{sel}$ allowing this solution is isolated (actually unique in the interval $(\sigma_{bottom}(\epsilon), \sigma_{top}(\epsilon))$). The condition on the sign of the derivative $\frac{dc(\hat{\sigma})}{d\hat{\sigma}^*}$ means that an increase of the stress at the interface above $\hat{\sigma}_{sel}$ produces a movement of the interface that decreases the size of the low shear rate band. Conversely, a decrease of the stress at the interface below $\hat{\sigma}_{sel}$ produces a displacement of the interface that increases the size of the low shear rate band. The same property can be found for other reaction-diffusion systems (e.g. the FitzHugh-Nagumo model of nerve conduction in biophysics) and has been occasionally referred to as “dominance principle” [35,36].

Remark 3. We have numerically checked this conjecture for various values of the parameter ϵ of the JS-d model (see next Section). All of these features are easy to prove for toy models that lead to integrable dynamical systems [22].

4.2 Numerical test of the conjecture

In order to test the conjecture for the JS-d model, and determine the relation between c and $\hat{\sigma}^*$ for different values of the unique parameter ϵ of the model in reduced variables, we have numerically integrated the following system of partial differential equations:

$$\partial_t S = \beta \partial_{\hat{r}}^2 S + c \sqrt{\beta} \partial_{\hat{r}} S - S + \frac{\sigma(\hat{r}) - S}{\epsilon} (1 - W) \quad (4.4a)$$

$$\partial_t W = \beta \partial_{\hat{r}}^2 W + c \sqrt{\beta} \partial_{\hat{r}} W - W + \frac{S(\sigma(\hat{r}) - S)}{\epsilon} \quad (4.4b)$$

with

$$S(L) = S^-(\sigma_{bottom}(\epsilon)), \quad S(-L) = S^+(\sigma_{top}(\epsilon)) \quad (4.4c)$$

$$W(L) = W^-(\sigma_{bottom}(\epsilon)), \quad W(-L) = W^+(\sigma_{top}(\epsilon)), \quad (4.4d)$$

where

$$\sigma(\hat{r}) = \sigma_{top}(\epsilon) + (\sigma_{bottom}(\epsilon) - \sigma_{top}(\epsilon)) \frac{r + L}{2L} \quad (4.5)$$

is conveniently chosen to scan the interval $[\sigma_{bottom}(\epsilon), \sigma_{top}(\epsilon)]$. Provided that the length L is taken much larger than the interface width, *i.e.* $\sqrt{\beta} \ll L$, the stationary solution is an interface in a position corresponding to a value of the stress equal to $\sigma^* = \hat{\sigma}^*(c)$. β can be interpreted as the diffusion coefficient and $\sigma(\hat{r})$ as the total stress inside the gap of width $2L$ although the applicability of the method does not rely on its connection to a concrete physical problem, but on its formal analogy to Eqs. (2.5) and (2.7), in the asymptotic $(L/\sqrt{\beta} \rightarrow \infty)$ limit.

In this way we determine $\sigma_{sel}(\epsilon) = \sigma^*(c = 0; \epsilon)$ and $\frac{dc}{d\sigma^*}(\sigma_{sel}; \epsilon) = \left(\frac{d\sigma}{dc}\right)^{-1}(c = 0; \epsilon)$. The first dependence will be used in calculating the flow curves in Section 5, while the sign of the latter constitutes a proof of the dominance principle.

In order to determine precisely the position of the stationary interface and hence the selected stress, we have solved Eqs. (4.4) for several values of β . Changing β modifies the interface width, analogous to a change of the diffusion coefficient, but does not alter the selected position of the interface for small β . The selected position of the interface and the corresponding value of the stress are given by the cross-over of several profiles obtained for different values of β as in Figs. 2a,b.

This algorithm is more convenient than the one used in [21] that considers a constant stress σ throughout the gap (planar shear) and tunes “by hand” the value of σ to obtain a stationary interface. Here the tuning of the stress is automatically obtained while integrating Eqs. (4.4).

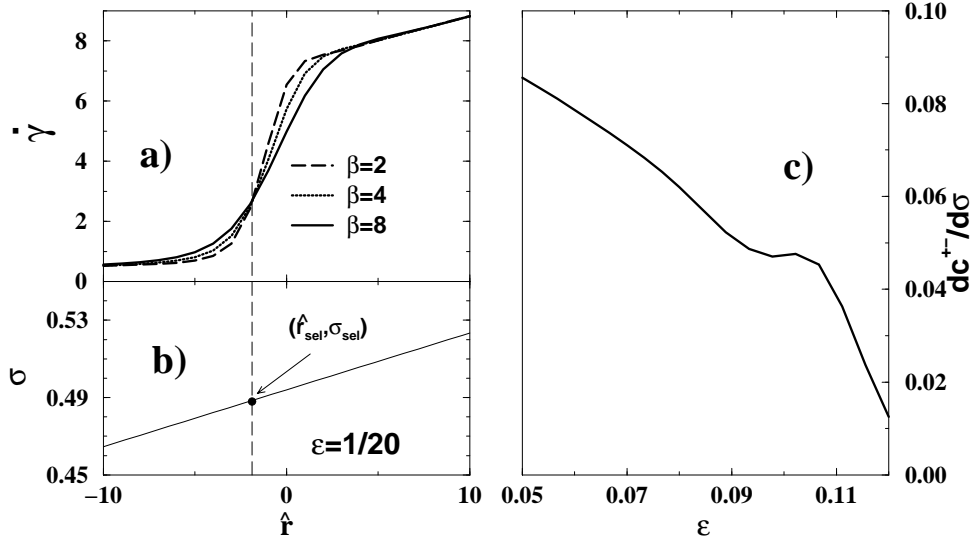


Fig. 2. a) Strain rate $\dot{\gamma}$ as a function of position for three different stationary solutions ($c = 0$) to Eq. (4.4) for $\beta = 2, 4, 8$. (b) Stress as a function of position. The cross-over of several stationary profiles gives the selected stress at the position noted by the vertical line. c) Derivative at $c^{+-} = 0$ of $c^{+-}(\hat{\sigma}^*)$ as a function of the retardation parameter ϵ , for an interface with the high shear rate band at its left. Here, $\sigma_{sel} = 0.4799$, compared to $\sigma_{sel} = 0.4827$ found in [21] for the JS model in planar Couette flow by a different method.

The selected value of the stress is compared with σ_{bottom} and σ_{top} in Fig. 1b and agrees with the result of the method in [21].

In order to test the dominance principle we have calculated $\frac{dc}{d\hat{\sigma}^*}$. Changing $\hat{r} \rightarrow -\hat{r}$ and $c \rightarrow -c$ leaves Eqs. (4.4) invariant. Thus if $c^{+-}(\hat{\sigma}^*)$ and $c^{-+}(\hat{\sigma}^*)$ are the velocities of the interface with the high shear rate at its left and right, respectively, then $c^{-+}(\hat{\sigma}^*) = -c^{+-}(\hat{\sigma}^*)$. Hence, our check that $\frac{dc^{+-}}{d\hat{\sigma}^*} > 0$, as shown in Fig. 2c, represents the sufficient test of the dominance principle.

4.3 Number of bands and stability of banded flow

The numerically tested conjecture implies that the interface is stationary in a position inside the gap where the value of the stress is $\hat{\sigma}_{sel}$. This position is unique ($\hat{r}_{sel} = (\hat{\Gamma}/\hat{\sigma}_{sel})^{1/2}$ for Couette flow, $\hat{r}_{sel} = \hat{\sigma}_{sel}/f$ for pipe flow) because in steady flow the total stress is monotonically dependent on the radius. Therefore, in Couette and pipe geometries banded flow has only one interface separating two bands. For Poiseuille slit flow, the dependence of the total stress on position is symmetric with respect to the middle of the slit, so there are two interfaces at $\hat{r}_{sel} = \pm \hat{\sigma}_{sel}/f$.

For both Poiseuille slit and pipe flow the sequence of bands is unique, with a centre low shear rate band and outer high shear rate bands (or an annular

band in pipe flow). In Couette flow, two sequences of bands are possible under certain conditions that we shall discuss in the next section. There are no restrictions on the sequence and order of the bands in planar flow because the total stress is constant throughout the gap; interfaces can exist anywhere, and any number and sequence of bands is possible, provided that the bands are much thicker than the interface width.

The stability of banded steady flow in presence of diffusion terms was tested in the Couette geometry by numerically evolving the dynamical equations [19] for both normal (high shear rate at the inner cylinder) and inverted sequences of bands. We have also proved (Appendix A) the stability of different types of banded solutions in Poiseuille and Couette flows with respect to perturbations of the position of the interface. A linear stability analysis for 1D perturbations around a banded profile, as well as the stability with respect to surface waves in 2D, involves lengthy functional analysis and will not be discussed here. Linear stability of banded flow for 1D perturbations in slit Poiseuille geometry was shown in Ref. [24] for a simplified model with only one order parameter. For the JS model (without diffusion) linear stability of the banded flow with any finite number of bands was proven in [15] for 1D perturbations in Poiseuille geometry, and possible instabilities induced by surface waves were discussed in [11].

Although linearly stable, the inverted sequence of bands is metastable because the interfaces separating a nucleus of low shear rate band within the high shear rate band will find themselves in a region of stress lower than $\hat{\sigma}_{sel}$ and according to the dominance principle will have non-zero velocities oriented such that the nucleus will grow [22]. The same is true for a nucleus of high shear rate band in the region where the total stress is higher than $\hat{\sigma}_{sel}$.

5 Applications of the results

5.1 Flow curves and extremities of branches

Flow curves can be obtained from Eqs. (3.5-3.8). These curves have several branches corresponding to homogeneous and banded flow. The extremities of different branches are fixed by the following conditions:

- (1) Homogeneous low shear rate flow is possible if

$$0 < \hat{\sigma}(\hat{r}) < \hat{\sigma}_{top}(\epsilon), \forall \hat{r} \quad (5.1)$$

(2) Homogeneous high shear rate flow is possible if

$$\hat{\sigma}(\hat{r}) > \hat{\sigma}_{bottom}(\epsilon), \forall \hat{r} \quad (5.2)$$

(3) Banded flow is possible if

$$\hat{\sigma}(\hat{r}_{sel}^*) = \hat{\sigma}_{sel} \quad (5.3)$$

for some position \hat{r}_{sel}^* inside the flow.

The sequence $(+-)$ is allowed if, in addition:

$$0 < \hat{\sigma}(\hat{r}) < \hat{\sigma}_{top}(\epsilon), \forall \hat{r}, \quad \hat{r} > \hat{r}_{sel}^* \quad (5.4)$$

$$\hat{\sigma}(\hat{r}) > \hat{\sigma}_{bottom}(\epsilon), \forall \hat{r}, \quad \hat{r} < \hat{r}_{sel}^* \quad (5.5)$$

while the sequence $(-+)$ is allowed if, in addition:

$$0 < \hat{\sigma}(\hat{r}) < \hat{\sigma}_{top}(\epsilon), \forall \hat{r}, \quad \hat{r} < \hat{r}_{sel}^* \quad (5.6)$$

$$\hat{\sigma}(\hat{r}) > \hat{\sigma}_{bottom}(\epsilon), \forall \hat{r}, \quad \hat{r} > \hat{r}_{sel}^* \quad (5.7)$$

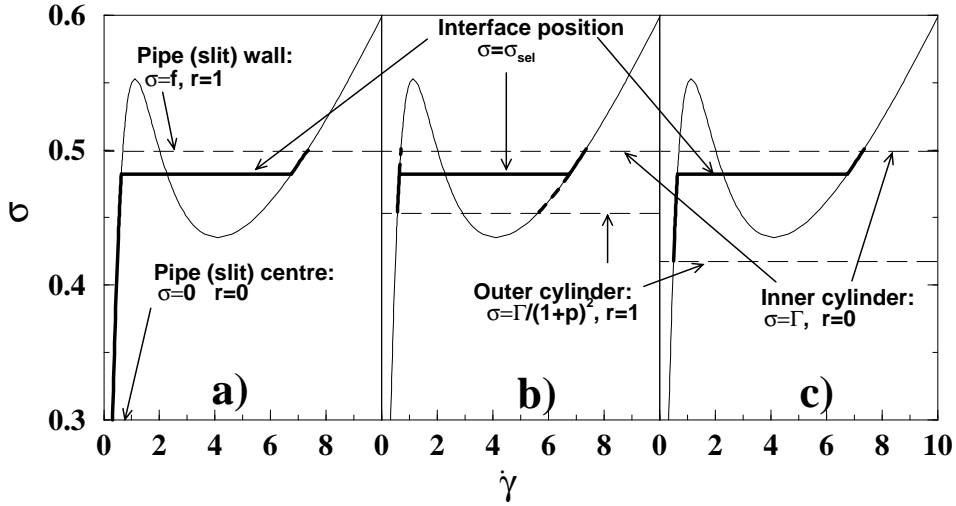


Fig. 3. Shear rate profiles (thick line) for banded flow (to each value of the total stress σ corresponds a position r inside the gap) in a) Poiseuille geometry, b) Couette geometry $p = 0.05, \epsilon = 1/20$ (region I of Fig. 5), with two possible sequences of bands ($(+-)$ solid, high shear rate band at the inner cylinder), and $(-+)$ dashed, high shear rate band at the outer cylinder), c) Couette geometry $p = 0.1, \epsilon = 1/20$ (region IV of Fig. 5 inverted sequence is not possible). The interface was considered of negligible width, hence it is represented by the segment $\sigma = \sigma_{sel}$.

In Poiseuille and Couette geometries, any banded steady flow profile can be conveniently represented as a segment on the local constitutive curve $\hat{\gamma}(\hat{\sigma})$, a solution of Eqs. (3.1) for variable stress $\hat{\sigma}$ (Fig. 3). Using the relation between \hat{r} and $\hat{\sigma}$ (Eqs. 2.6b, 2.9, 2.12) one can map a steady state $\hat{\gamma}(\hat{r})$ onto a segment

of the local constitutive curve $\hat{\gamma}(\hat{\sigma})$ for stresses $0 < \hat{\sigma} < f$ (Poiseuille), or $\hat{\Gamma}/(1+p)^2 < \hat{\sigma} < \hat{\Gamma}$ (Couette). The outer layer solution lies on the local constitutive curve, while the inner layer solution is a horizontal segment at $\hat{\sigma} = \hat{\sigma}_{sel}$, corresponding to a small width interface.

5.1.1 Planar shear

The equation of the low shear rate branch is $\hat{V} = \hat{\gamma}^-(\hat{\sigma})$, with $0 < \hat{\sigma} < \hat{\sigma}_{top}(\epsilon)$, and the high shear branch can be described as $\hat{V} = \hat{\gamma}^+(\hat{\sigma})$, with $\hat{\sigma}_{bottom}(\epsilon) < \hat{\sigma}$. The banded flow corresponds to the plateau $\hat{\sigma} = \hat{\sigma}_{sel}$. The homogeneous branches of the flow curve are on the local constitutive curve represented in Fig. 1.

5.1.2 Poiseuille flow

The low shear rate branch can be obtained from Eq. (3.5) by choosing $\hat{\sigma}^* = f$ (interface near the wall at $\hat{r}^* = 1$), and according to Eq. (5.1) with the restriction $0 < f < \hat{\sigma}_{top}(\epsilon)$. The unique banded profile $(-+)$ (low shear rate at $\hat{r} = 0$) is described by Eq. (3.5), choosing $\hat{\sigma}^* = \hat{\sigma}_{sel}$, according to Eq. (5.3) with the restriction $f = \hat{\sigma}_{sel}(\epsilon)/\hat{r}_{sel}^* > \hat{\sigma}_{sel}(\epsilon)$. Then Eq. (5.7) is automatically fulfilled because it becomes equivalent to $\sigma_{bottom}(\epsilon) < \hat{\sigma}_{sel}(\epsilon) < \sigma_{top}(\epsilon)$, that is true for $\epsilon < 1/8$ (actually for all values of ϵ for which the local constitutive curve is nonmonotonic, Fig. 1). Eq. (5.5) is not fulfilled (thus the inverted sequence of bands is forbidden) because it becomes equivalent to $f\hat{r} > \sigma_{bottom}, \forall \hat{r} < \hat{r}_{sel}^*$, obviously not true for $\hat{r} = 0$. The banded branch continues until $f = \infty$ and $\hat{r}^* = 0$. The low shear rate band is continuously squeezed until it disappears in the limit $f = \infty$. Thus, the flow curve has no high shear rate branch, because the high shear rate band occupies the entire volume only at $f = \infty$. The flow curve in this geometry is represented in Fig. 4a for different retardation parameters ϵ .

5.1.3 Cylindrical Couette flow

In Couette flow Eq. (5.5) is always fulfilled and the normal sequence $(-+)$ of bands is allowed for all shear rates along the plateau (see Fig. 3b-d). Nevertheless, the inverted sequence $(-+)$ is not allowed for the values of Γ, p, ϵ when the total stress at the inner cylinder is higher than σ_{top} , or when the total stress at the outer cylinder is lower than σ_{bottom} , see Fig. 3c. A detailed analysis of this condition given in Appendix B shows the existence of five possibilities and regions in the plane of parameters (p, ϵ) , explained in Fig. 5.

Some examples of flow curves in the Couette geometry are presented in Fig. 4.

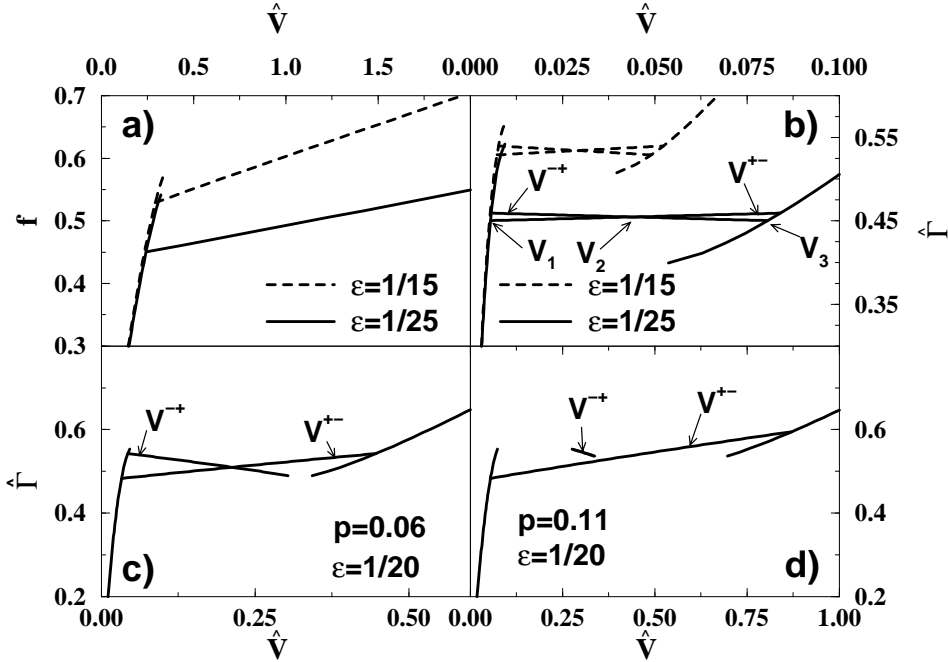


Fig. 4. Flow curves in reduced variables for a) Poiseuille flow, b-d) Couette geometry with $p = 0.01$ (b), $p = 0.06$ (c), and $p = 0.11$ (d). For Couette flow, V^{+-} and V^{-+} correspond to flow curves with the high strain rate band near the inner and outer cylinders, respectively. (b) and (c) correspond to Regions I and II, while (d) corresponds to Region IV in Fig. 5.

Eq. (A.8a) implies that the branch $(+-)$ has a positive slope $\frac{\partial \hat{\Gamma}}{\partial \hat{V}} > 0$, while Eq. (A.8b) implies that the branch $(-+)$ has a negative slope $\frac{\partial \hat{\Gamma}}{\partial \hat{V}} < 0$. The latter does not imply a mechanical instability, because any mechanical drift is constrained by the imposed mean shear rate. Furthermore, the stability of this sequence of bands is shown by our numerical simulations [19] and by the stability analysis with respect to the position of the interface (Appendix A). As suggested in [16,17], stability of banded flow is not directly connected to the slope of the flow curve, but rather to the slope of the local constitutive curve of the homogeneous bands; if the latter is negative for at least one band (intermediate branch in Fig. 1a), then the flow is unstable.

Fig. 4b corresponds to values of the parameters (p, ϵ) chosen in Region I of Fig. 5, with both sequences of bands allowed. Fig. 4c corresponds to parameters chosen in Region II (the inverted band sequence is forbidden at higher strain rates), while Fig. 4d corresponds to parameters chosen in Region IV (shear rates allowing the existence of the inverted sequence are limited both at upper and lower values). Interestingly, the branch corresponding to the inverted band sequence no longer crosses the normal band sequence branch for $p = 0.11, \epsilon = 0.05$ in Fig. 4d. Note that the “plateau” in the banded region is steeper (larger $d\hat{\Gamma}/d\hat{V}$) for a more highly curved geometry (larger p).

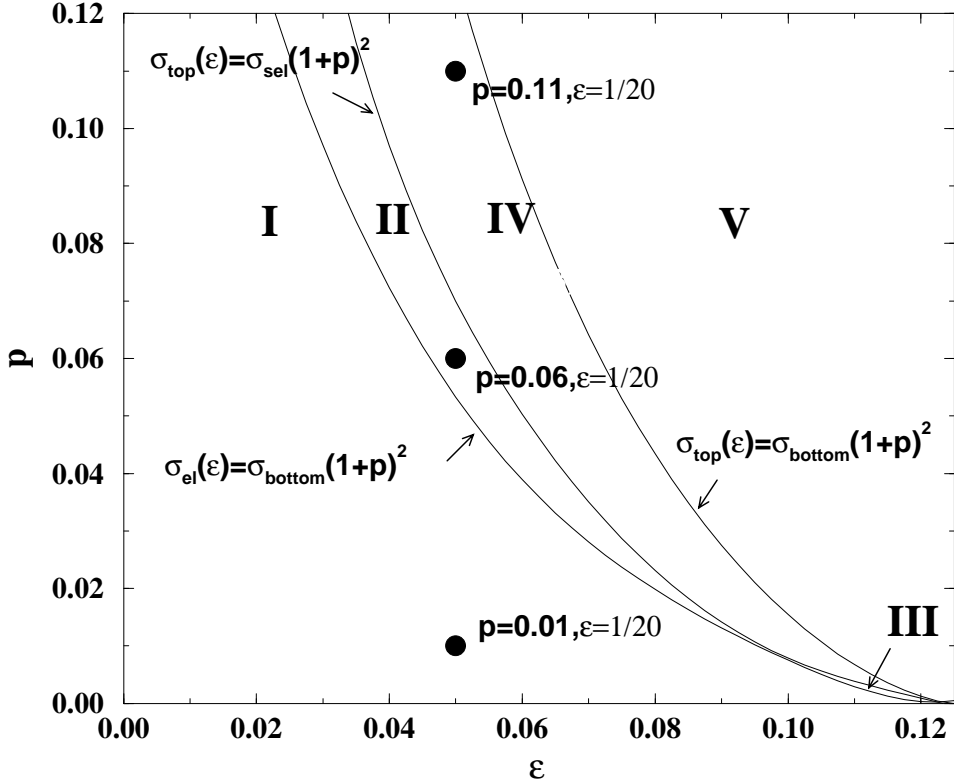


Fig. 5. Existence conditions for the inverted sequence of bands in Couette flow, separating 5 regions I-V in the plane (ϵ, p) . The dots \bullet correspond to the flow curves in Fig. 4. Inverted bands are only possible in Regions I (for all shear rates along the plateau), II (for a domain of shear rates truncated at the right end of the plateau), III (for a domain of shear rates truncated at the left end of the plateau), and IV (for a domain of shear rates truncated at both ends of the plateau).

The various dangling segments corresponding to different branches of the flow curves may be the origin of hysteresis phenomena. Part of these phenomena were described in a previous paper [19] using numerical integration of the dynamical equations. We have shown there that some segments of the flow curve can be reached only by special experimental scenarios. This is in agreement with the results of this work. For instance, starting from rest in Fig. 4b, when $\epsilon = 1/25$, the system can first reach the branch $(+-)$ within the interval of gap velocities $\hat{V}_1 < \hat{V} < \hat{V}_2$ and the branch $(-+)$ within the interval $\hat{V}_2 < \hat{V} < \hat{V}_3$ (Fig. 4b). In order to reach other parts of the banded branches one must, for example, prepare the system with a given band sequence and then adiabatically change the value of the gap velocity in order to scan the entire length of the branch. This is possible for $p < 0.1$ for both bands $(+-)$, but for $p = 0.11$ in Fig. 4d all start-up preparations of the flow end with the sequence $(+-)$ and it is impossible to reach the isolated branch $(-+)$. Numerically one could start from rest with a smaller value of p , reaching thus the $(-+)$ branch, and then change p adiabatically, but this is not a conceivable experimental procedure.

5.2 Interface Width

Linearising Eqs. (3.3) at $\tilde{r} = \pm\infty$ we obtain

$$\partial_{\tilde{r}}^2 \begin{pmatrix} \delta\hat{S}_{in} \\ \delta\hat{W}_{in} \end{pmatrix} = \mathbf{M}^\pm \begin{pmatrix} \delta\hat{S}_{in} \\ \delta\hat{W}_{in} \end{pmatrix} \quad (5.8)$$

where $\delta\hat{S}_{in}, \delta\hat{W}_{in}$ are small deviations of stresses with respect to asymptotic steady values and

$$\mathbf{M}^\pm(\hat{\sigma}_{sel}) = \begin{pmatrix} 1 - [1 - \hat{W}^\pm(\hat{\sigma}_{sel})]/\epsilon & [\hat{\sigma}_{sel} - \hat{S}^\pm(\hat{\sigma}_{sel})]/\epsilon \\ [\hat{\sigma}_{sel} - 2\hat{S}^\pm(\hat{\sigma}_{sel})]/\epsilon & 1 \end{pmatrix} \quad (5.9)$$

Asymptotically, the interface profile can be approximated by a combination of exponentials, and the widths of the interface towards the high shear rate band w^+ and towards the low shear rate band w^- are the characteristic decay lengths of the slowest of the exponentials on the two sides of the interface, related to the eigenvalues of \mathbf{M}^\pm :

$$w^\pm = \frac{\sqrt{\mathcal{D}\tau}}{\min_{i=1,2} \left\{ \text{Re} \left(\sqrt{\chi_i^\pm(\hat{\sigma}^*, \epsilon)} \right) \right\}} \quad (5.10)$$

where $i = 1, 2$ correspond to the two eigenvalues $\chi_{1,2}^-$ of \mathbf{M}^- and to the two eigenvalues $\chi_{1,2}^+$ of \mathbf{M}^+ (see Fig. 6a). The dependence of the interface width on the retardation parameter ϵ is shown in Fig. 6b. The interface is asymmetric (thicker in the low shear rate band).

The non-vanishing imaginary parts of $\sqrt{\chi_{1,2}^\pm}$ imply damped oscillations of the interface profile towards the high shear rate band. The wavelength of these oscillations is the inverse of $|\text{Im}\sqrt{\chi_i^\pm}|$ and because $|\text{Im}\sqrt{\chi_i^\pm}| < \text{Min}(\text{Re}\sqrt{\chi_i^\pm})$ (Fig. 6a) the width of the interface is smaller compared to this wavelength the overdamped oscillations are hardly noticeable in Fig. 2a showing the interface profile.

As seen in Fig. 6a, a bifurcation occurs for low polymer viscosity. For $\epsilon > 0.1$, the eigenvalues $\chi_{1,2}^\pm$ are no longer complex conjugate ($\text{Re}\chi_1^\pm \neq \text{Re}\chi_2^\pm$). This bifurcation produces a discontinuity of the first derivative of $w^+(\epsilon)$ at $\epsilon = 0.1$. At the same time the imaginary parts of $\chi_{1,2}^\pm$ vanish. This particularity of the JS model was also noticed in [14]. At $\epsilon = 1/8$, which is the limit of existence of banded solutions (above $\epsilon = 1/8$ the local constitutive curve is monotonic) χ_1^-, χ_1^+ vanish, therefore both widths w^\pm diverge, Fig. 6b.

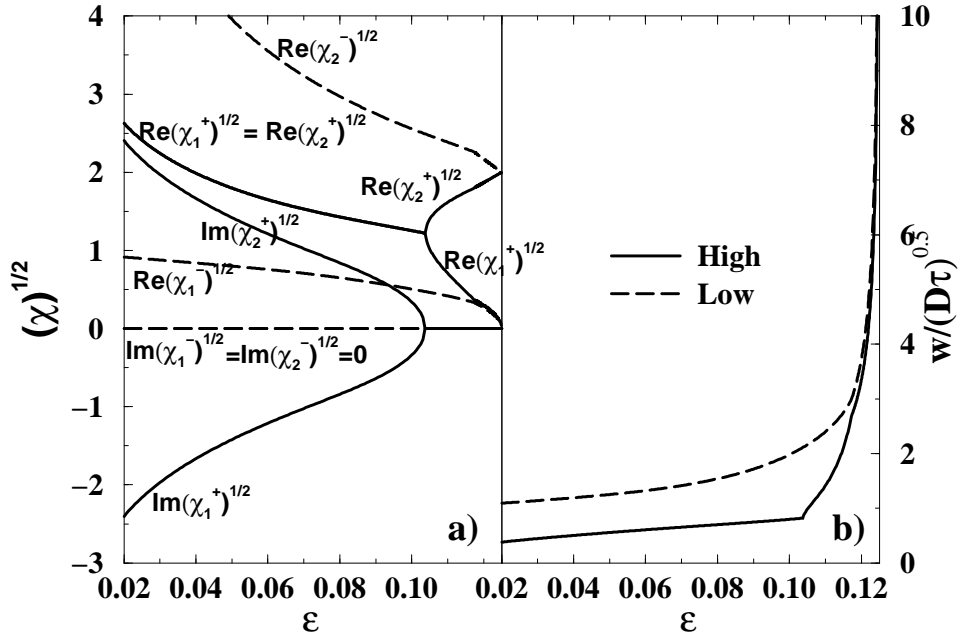


Fig. 6. (a) Eigenvalues of $\mathbf{M}^\pm(\sigma_{sel})$ the matrix of the linearised steady flow equations, for the high (+) and low (-) shear rate bands and (b) interface width on the high or low shear rate side of the interface, as a function of the retardation parameter ϵ .

The interface width scales like $\sqrt{D\tau}$, which is typically of the same order as the polymer chain size [22]. The prefactor can be rather big for small polymer viscosity (it diverges at the critical point $\epsilon = 1/8$ like $(1/8 - \epsilon)^{-1/2}$) and it is geometry independent. Thus, the width of a thin, steady interface should be the same in planar shear, as in Poiseuille and Couette flows for any curvature. Ref. [30] determined the width of the interface for micelles experiments in cone and plate geometry, and reported an increase in width of a factor 3 when the cone-plate angle changes from 4° to 7° . Although we did not investigate this particular geometry here, we expect that rather generally the width of a thin, steady interface depends only on the constitutive model and does not depend on the geometry. The widths reported in [30] are much larger than the polymer chain size, therefore they are most probably produced by a different mechanism. A possible explanation is the dynamical broadening due to travelling surface waves in two-layer flows [37,38].

6 Conclusions

We have discussed the steady banded flow of the Johnson-Segalman model, considering 1D shear rate profiles in Poiseuille, cylindrical Couette and planar shear geometries, under controlled shear rate conditions. The introduction of

a non-local diffusion term in the JS local constitutive relation lifts the continuous degeneracy and the history dependence of the steady flow solution for Poiseuille and cylindrical Couette geometries, and generally for any geometry that imposes a non-uniform total shear stress. In order to analyse these phenomena we used matched asymptotic techniques which are common in the field of reaction-diffusion systems describing processes like combustion or nerve conduction, but which, to our knowledge, are new in the field of creeping flow of complex fluids. The use of the JS model in this paper should be considered only as an example of application of these methods in order to investigate the consequences of diffusion terms on banded flow.

We showed that in Poiseuille and cylindrical Couette geometries steady banded flow has two bands, which seems to be the case in birefringence experiments [31,32]. NMR visualisation of more than two bands as reported in Ref. [29] in the Couette geometry could be due to slowly decaying (or pinned) transients. Note that the speed of a moving interface scales as $D^{1/2}$. Another possibility, not taken into account here but that needs further investigation, is that concentration effects may stabilise banded flows with more than two bands. Thus, a depletion layer at the inner cylinder increases locally the selected stress and may equilibrate a second interface closer to the inner cylinder than the first equilibrium position which corresponds to higher concentration and lower selected stress.

In the absence of diffusion steady banded flow can form any number of bands. The same arbitrariness of the number of bands was shown in steady Poiseuille flow [16,17]. In numerical simulations of Ref. [25] no selection was noticed, except for the one imposed by the mesh size. Recently, we showed numerically [19] that even in Couette flow, solving the flow in the absence of diffusion is an ill-posed problem, unstable to noise in the initial conditions. The lack of robustness of the flow increases when the curvature decreases, in the sense that larger and larger regions inside the gap may split into multiple bands under perturbations of the initial conditions. Refs. [12,39] found a unique, single interface solution even in the planar shear of the JS model without a diffusion term, although this interface has a finite width that suggests diffusion terms intrinsic to the finite element scheme. With diffusion the system of dynamical equations becomes parabolic leading to compactness of the global attractors and to stability with respect to initial conditions [24].

In certain conditions in cylindrical Couette flow (low curvature and high polymer viscosity), both normal and inverted band sequences are allowed for the same shear rate. Nevertheless, the inverted band is metastable and can be reached from rest only on the second half of the plateau [19]. Although this branch has not been observed experimentally, its existence and linear stability is proven rigorously and may have consequences on the kinetics of shear-banding within a restricted domain of control parameters.

An interesting feature shown by experimental flow curves and reproduced by our theoretical model is the presence of a selected stress plateau, reminiscent of isotherms at liquid-gas or decompositions of binary systems first order phase transitions. In thermodynamic transitions the plateau is fixed by a Maxwell type construction, justified by the equality of the chemical potentials of the coexisting phases. In the model we present here the equilibrium of "phases" is a condition of existence of a stationary interface, and relies on the balance between stress diffusion across the interface and non-linear stress relaxation. The retardation parameter plays the rôle of temperature, and its critical value $\epsilon = 1/8$ is analogous to an equilibrium critical point. The extremities of the plateau for varying ϵ describe a curve that is analogous to a binodal for phase separation, the critical point being the top of the binodal (Fig. 1a). As in first order transitions the width of the interface separating the two bands diverges at the critical point. Whether the studied phenomena have more than a formal connection to thermodynamics is still an open question.

Apart from settling some basic questions concerning how the presence of diffusion terms affects measurable flow curves, we hope that the results presented here will stimulate more accurate and diversified experiments, eventually searching for various unusual features such as inverted band sequences and the special kinetic pathways involved. This could be a test of the theoretical assumptions but could also increase the operational range in view of possible applications.

Acknowledgements

We thank T.C.B. McLeish and C.-Y. D. Lu for useful discussions. This work is funded by EPSRC (GR/L70455).

A Stability of the flow with respect to changes in the position of the interface

Stability with respect to the position of the interface means that any displacement $\delta\hat{r}^*$ of the interface leads to a moving interface solution with velocity oriented towards the equilibrium position \hat{r}_{sel} , *i.e.*:

$$c[\hat{\sigma}(\hat{r}_{sel} + \delta\hat{r}^*)]\delta\hat{r}^* = \left. \frac{dc}{d\hat{\sigma}} \right|_{\hat{\sigma}_{sel}} \left. \frac{\partial\hat{\sigma}}{\partial\hat{r}^*} \right|_{\hat{v}} (\delta\hat{r}^*)^2 < 0 \quad (\text{A.1})$$

The partial derivative occurring in Eq. (A.1) can be obtained as

$$\left. \frac{\partial \hat{\sigma}^*}{\partial \hat{r}^*} \right|_{\hat{V}} = - \frac{\left. \frac{\partial \hat{V}}{\partial \hat{r}^*} \right|_{\hat{\sigma}^*}}{\left. \frac{\partial \hat{V}}{\partial \hat{\sigma}^*} \right|_{\hat{r}^*}} \quad (\text{A.2})$$

Using Eqs. (A.2, 3.5, 2.6b) for Poiseuille flow we obtain:

$$\left. \frac{\partial \hat{V}}{\partial f} \right|_{\hat{\sigma}^*} = \frac{\hat{\gamma}^+(f) - \hat{V}}{f} \quad (\text{A.3})$$

$$\left. \frac{\partial \hat{\sigma}^*}{\partial \hat{r}^*} \right|_{\hat{V}} = \frac{- \left. \frac{\partial \hat{V}}{\partial f} \right|_{\hat{\sigma}^*} \left. \frac{\partial f}{\partial \hat{r}^*} \right|_{\hat{\sigma}^*}}{\left. \frac{\partial \hat{V}}{\partial \hat{\sigma}^*} \right|_f + \left. \frac{\partial \hat{V}}{\partial f} \right|_{\hat{\sigma}^*} \left. \frac{\partial f}{\partial \hat{\sigma}^*} \right|_{\hat{r}^*}} = \frac{f}{1 - P(f, \hat{\sigma}_{sel})} \quad (\text{A.4})$$

where

$$P(f, \hat{\sigma}_{sel}) = \frac{\hat{\sigma}_{sel} [\hat{\gamma}^+(\hat{\sigma}_{sel}) - \hat{\gamma}^-(\hat{\sigma}_{sel})]}{f [\hat{\gamma}^+(f) - \hat{V}(\hat{\sigma}_{sel}, f)]} \quad (\text{A.5})$$

According to the tested conjecture, an increase of the total stress will displace the interface towards the middle of the slit or pipe ($\frac{dc}{d\hat{\sigma}} < 0$), so using Eq. (A.4) the stability condition (A.1) for plug flow in Poiseuille geometry reads:

$$P(f, \hat{\sigma}_{sel}) < 1. \quad (\text{A.6})$$

Using the fact that $\hat{\gamma}^-(\hat{\sigma})$ is an increasing function of $\hat{\sigma}$ it follows from Eq. (3.5) that $\hat{V}(\hat{\sigma}_{sel}, \hat{\sigma}_{sel}) < \hat{\gamma}^-(\hat{\sigma}_{sel}) < \hat{\gamma}^+(\hat{\sigma}_{sel})$ and therefore $P(\hat{\sigma}_{sel}, \hat{\sigma}_{sel}) < 1$. $P(f, \hat{\sigma}_{sel})$ is a monotonically decreasing function of f , provided that $\hat{\gamma}^+(\hat{\sigma})$ is increasing with $\hat{\sigma}$, as shown by

$$\left. \frac{\partial P}{\partial f} \right|_{\hat{\sigma}_{sel}} = - \frac{d\hat{\gamma}^+(f)}{df} \left[\frac{P}{\hat{\gamma}^+(f) - \hat{V}(\hat{\sigma}_{sel}, f)} \right] < 0. \quad (\text{A.7})$$

Because the lowest allowed value of f for banded flow is $f = \hat{\sigma}_{sel}$, the stability criterion is always satisfied.

A similar stability analysis can be performed in the case of the cylindrical

Couette flow. Using Eqs. (A.2), (3.6), (3.7), (2.9) for Couette flow we obtain:

$$\left. \frac{\partial \hat{V}^{+-}}{\partial \Gamma} \right|_{\hat{\sigma}^*} = \frac{\hat{\gamma}^+(\Gamma) - \hat{\gamma}^-(\Gamma/(1+p)^2)}{2\Gamma} \quad (\text{A.8a})$$

$$\left. \frac{\partial \hat{V}^{-+}}{\partial \Gamma} \right|_{\hat{\sigma}^*} = \frac{-\hat{\gamma}^+(\Gamma/(1+p)^2) + \hat{\gamma}^-(\Gamma)}{2\Gamma} \quad (\text{A.8b})$$

$$\left. \frac{\partial \hat{\sigma}^*}{\partial \hat{r}^*} \right|_{\hat{V}^{+-}} = \frac{-4\hat{\Gamma}^{-1/2}\hat{\sigma}_{sel}^{3/2}}{1 - C^{+-}(\hat{\Gamma}, \hat{\sigma}_{sel}, p)} \quad (\text{A.8c})$$

$$\left. \frac{\partial \hat{\sigma}^*}{\partial \hat{r}^*} \right|_{\hat{V}^{-+}} = \frac{-4\hat{\Gamma}^{-1/2}\hat{\sigma}_{sel}^{3/2}}{1 - C^{-+}(\hat{\Gamma}, \hat{\sigma}_{sel}, p)}, \quad (\text{A.8d})$$

with

$$C^{+-}(\hat{\Gamma}, \hat{\sigma}_{sel}, p) = \frac{\hat{\gamma}^+(\hat{\sigma}_{sel}) - \hat{\gamma}^-(\hat{\sigma}_{sel})}{\hat{\gamma}^+(\hat{\Gamma}) - \hat{\gamma}^-(\hat{\Gamma}/(1+p)^2)} \quad (\text{A.8e})$$

$$C^{-+}(\hat{\Gamma}, \hat{\sigma}_{sel}, p) = \frac{\hat{\gamma}^+(\hat{\sigma}_{sel}) - \hat{\gamma}^-(\hat{\sigma}_{sel})}{\hat{\gamma}^+(\hat{\Gamma}/(1+p)^2) - \hat{\gamma}^-(\hat{\Gamma})}, \quad (\text{A.8f})$$

where the sequence $+-$ refers to the high shear rate band near the inner cylinder and the sequence $-+$ refers to the high shear rate band near the outer cylinder.

The stability criteria for the two sequences are respectively:

$$C^{+-}(\hat{\Gamma}, \hat{\sigma}_{sel}, p) < 1 \quad (\text{A.9a})$$

$$C^{-+}(\hat{\Gamma}, \hat{\sigma}_{sel}, p) > 1 \quad (\text{A.9b})$$

Because $\hat{\Gamma}/(1+p)^2 < \hat{\sigma}_{sel} < \hat{\Gamma}$, and provided that both $\hat{\gamma}^-(\hat{\sigma})$, and $\hat{\gamma}^+(\hat{\sigma})$ are increasing functions of the total stress $\hat{\sigma}$, the stability criteria are always fulfilled for both sequences of bands.

To conclude, banded flow is stable with respect to displacements of the interface in Poiseuille slit and pipe geometry. In cylindrical Couette flow, both sequences of bands are stable with respect to displacements of the interface, provided that their existence is allowed by further criteria discussed in Appendix B.

B Existence conditions for band sequences in cylindrical Couette geometry

The homogeneous low shear rate branch is obtained from Eq. (3.6) with $\hat{\sigma}^* = \hat{\Gamma}$ (interface at the inner wall $\hat{r}^* = 1$), and according to Eq. (5.1) with the restriction $0 < \hat{\Gamma}/\hat{r}^2 < \sigma_{top}(\epsilon), \forall \hat{r} \in (1, 1+p)$, which is equivalent to $0 < \hat{\Gamma} < \hat{\sigma}_{top}(\epsilon)$. The high shear rate branch can be obtained from Eq. (3.6) with $\hat{\sigma}^* = \hat{\Gamma}/(1+p)^2$ (interface at the outer wall $\hat{r}^* = 1+p$), and according to Eq. (5.2) with the restriction $\hat{\Gamma}/\hat{r}^2 > \sigma_{top}(\epsilon), \forall \hat{r} \in (1, 1+p)$, i.e $\hat{\Gamma} > (1+p)^2 \hat{\sigma}_{bottom}(\epsilon)$.

Banded flow with the two possible band sequences is described by Eqs. (3.6, 3.7) with $\hat{\sigma}^* = \hat{\sigma}_{sel}$. Eq. (5.3) imposes the limiting values of the torque:

$$\hat{\sigma}_{sel} < \hat{\Gamma} = \hat{\sigma}_{sel}(\hat{r}_{sel}^*)^2 < \hat{\sigma}_{sel}(1+p)^2 \quad (\text{B.1})$$

The two limiting values correspond to the steady interface touching the inner ($\hat{r}_{sel}^* = 1$) and the outer ($\hat{r}_{sel}^* = 1+p$) cylinder, respectively.

If Eq. (5.3) is fulfilled, Eq. (5.5) is automatically fulfilled because it becomes equivalent to $\sigma_{bottom}(\epsilon) < \sigma_{sel}(\epsilon) < \sigma_{top}(\epsilon)$. Thus the sequence of bands (+-) (high shear rate band at the inner cylinder) exists for all torque values such that:

$$\hat{\Gamma} \in I_{\Gamma}^s := (\hat{\sigma}_{sel}, \hat{\sigma}_{sel}(1+p)^2). \quad (\text{B.2})$$

If Eq. (5.3) is fulfilled, the condition 5.7 becomes equivalent to:

$$\hat{\Gamma} \in I_{\Gamma} := ((1+p)^2 \hat{\sigma}_{bottom}, \hat{\sigma}_{top}), \quad (\text{B.3})$$

hence the (-+) sequence of bands (high shear rate band at the outer cylinder) exists for torques $\hat{\Gamma} \in I_{-+} = I_{\Gamma}^s \cap I_{\Gamma}$. The interval I_{-+} can be either empty, or strictly included in I_{Γ}^s , or coincide with I_{Γ}^s . There are several regions in the plane of parameters (ϵ, p) , corresponding to these situations.

- (I) $\hat{\sigma}_{bottom}(\epsilon)(1+p)^2 < \hat{\sigma}_{sel}, \hat{\sigma}_{top}(\epsilon) > \hat{\sigma}_{sel}(1+p)^2, \hat{\sigma}_{bottom}(\epsilon)(1+p)^2 < \hat{\sigma}_{top}(\epsilon)$.
In this region both band sequences are allowed for torques in the full interval I_{Γ}^s because $I_{\Gamma}^s \subset I_{\Gamma}$ and therefore $I_{-+} = I_{\Gamma}^s$.
- (II) $\hat{\sigma}_{bottom}(\epsilon)(1+p)^2 > \hat{\sigma}_{sel}, \hat{\sigma}_{top}(\epsilon) > \hat{\sigma}_{sel}(1+p)^2, \hat{\sigma}_{bottom}(\epsilon)(1+p)^2 < \hat{\sigma}_{top}(\epsilon)$. In this region the sequence (+-) is allowed for torques within I_{Γ}^s , while the sequence (-+) is allowed in the interval $I_{-+} = (\hat{\sigma}_{bottom}(\epsilon)(1+p)^2, \hat{\sigma}_{sel}(\epsilon)(1+p)^2)$ obtained by truncating I_{Γ}^s at its low stress limit.
- (III) $\hat{\sigma}_{bottom}(\epsilon)(1+p)^2 < \hat{\sigma}_{sel}, \hat{\sigma}_{top}(\epsilon) < \hat{\sigma}_{sel}(1+p)^2, \hat{\sigma}_{bottom}(\epsilon)(1+p)^2 < \hat{\sigma}_{top}(\epsilon)$. In this region the sequence (+-) is allowed for torques within I_{Γ}^s , while the sequence (-+) is allowed in the interval $I_{-+} = (\hat{\sigma}_{sel}(\epsilon), \hat{\sigma}_{top}(\epsilon))$ obtained by truncating I_{Γ}^s at its high stress limit.

- (IV) $\hat{\sigma}_{bottom}(\epsilon)(1+p)^2 > \hat{\sigma}_{sel}$, $\hat{\sigma}_{top}(\epsilon) < \hat{\sigma}_{sel}(1+p)^2$, $\hat{\sigma}_{bottom}(\epsilon)(1+p)^2 < \hat{\sigma}_{top}(\epsilon)$.
 In this region the sequence $(+-)$ is allowed for torques within I_{Γ}^s , while the sequence $(-+)$ is allowed in the interval $I_{-+} = (\hat{\sigma}_{bottom}(\epsilon)(1+p)^2, \hat{\sigma}_{top}(\epsilon))$ is obtained by truncating I_{Γ}^s at both limits.
- (V) $\hat{\sigma}_{bottom}(\epsilon)(1+p)^2 > \hat{\sigma}_{sel}$, $\hat{\sigma}_{top}(\epsilon) < \hat{\sigma}_{sel}(1+p)^2$, $\hat{\sigma}_{bottom}(\epsilon)(1+p)^2 > \hat{\sigma}_{top}(\epsilon)$.
 In this region the sequence $(+-)$ is allowed for torques within I_{Γ}^s , while the sequence $(-+)$ is forbidden for all values of the torque, because $I_{-+} = \emptyset$.

These five regions are shown in Fig. 5. Region III is very narrow, and practically represents the frontier between the Regions I and IV. In general, for given Γ and ϵ the inverted band sequence is forbidden for sufficiently highly curved geometries (large enough p). A less formal approach to obtain the same results is shown in Fig. 3. Fig. 3c corresponds to the case of large curvature (region IV), in which the value of the stress does not allow for the existence of the low shear rate band at the outer cylinder forbidding thus the sequence $(-+)$, because $\Gamma/(1+p)^2 < \sigma_{bottom}$. For small curvature (Fig. 3b) the values of the stress at the inner and outer cylinders allow the existence of both high and low shear rate bands, thus both sequences of bands can exist. The possibility of an inverted band sequence was also found in Ref. [40] for a two fluid model of shear banding in polymer blends.

References

- [1] H. Hoffmann, G. Platz, H. Rehage, W. Schorr, and W. Ulbricht, Viskoelastische Tensidlösungen, Ber. Bunsenges. Phys. Chem., 85 (1981) 255-266.
- [2] J. F. Berret, D. C. Roux, and G. Porte, Isotropic-to-nematic transition in wormlike micelles under shear, J. Phys. II (France), 4 (1994) 1261-1279.
- [3] P. T. Callaghan, M. E. Cates, C. J. Rofe, and J. A. F. Smeulders, A study of the spurt effect in wormlike micelles using nuclear-magnetic-resonance microscopy, J. Phys. II (France), 6 (1996) 375-393.
- [4] C. Grand, J. Arrault, and M. E. Cates, Slow transients and metastability in wormlike micelle rheology, J. Phys. II (France), 7 (1997) 1071-1086.
- [5] P. Boltenhagen, Y. T. Hu, E. F. Matthys, and D. J. Pine, Observation of bulk phase separation and coexistence in a sheared micellar solution, Phys. Rev. Lett., 79 (1997) 2359-2362.
- [6] P. Terech, Fibers and wires in organogels from low-mass compounds: typical structural and rheological properties, Ber. Bunsenges. Phys. Chem., 102 (1998) 1630-1643.
- [7] D. Bonn, J. Meunier, O. Greffier, A. Alkhwaji, and H. Kellay, Bistability in non-Newtonian flow: rheology of lyotropic liquid crystals, Phys. Rev., 58 (1998) 2115-2118.

- [8] M. Johnson and D. Segalman, A model for viscoelastic fluid behavior which allows non-affine deformation, *J. Non-Newt. Fl. Mech*, 2 (1977) 255-270.
- [9] M. Doi and S. F. Edwards, *The Theory of Polymer Dynamics* (Clarendon, Oxford, 1989).
- [10] T. C. B. McLeish and R. C. Ball, A molecular approach to the spurt effect in polymer melt flow, *J. Poly. Sci. B-Poly. Phys.*, 24 (1986) 1735-1745.
- [11] Y. Y. Renardy, Spurt and instability in a two-layer Johnson-Segalman liquid, *The. Comp. Fl. Dyn.*, 7 (1995) 463-475.
- [12] P. Español, X. F. Yuan, and R. C. Ball, Shear banding flow in the Johnson-Segalman fluid, *J. Non-Newt. Fl. Mech.*, 65 (1996) 93-109.
- [13] D. S. Malkus, J. S. Nohel, and B. J. Plohr, Dynamics of shear flow of a non-Newtonian fluid, *J. Comp. Phys.*, 87 (1990) 464-487.
- [14] D. S. Malkus, J. S. Nohel, and B. J. Plohr, Analysis of new phenomena in shear flow of non-Newtonian fluids, *SIAM J. Appl. Math.*, 51 (1991) 899-929.
- [15] J. S. Nohel, R. L. Pego, and A. E. Tzavaras, Stability of discontinuous steady states in shearing motions of a non-Newtonian fluid, *Proc. Roy. Soc. Edin.*, 115A (1990) 39-59.
- [16] G. C. Georgiou and D. Vlassopoulos, On the stability of the simple shear flow of a Johnson-Segalman fluid, *J. Non-Newt. Fl. Mech.*, 75 (1998) 77-79.
- [17] M. M. Fyrillas, G. C. Georgiou, and D. Vlassopoulos, Time-dependent plane Poiseuille flow of a Johnson-Segalman fluid, *J. Non-Newt. Fl. Mech.*, 82 (1999) 105-123.
- [18] F. Greco and R. C. Ball, Shear-band formation in a Non-Newtonian fluid model with a constitutive instability, *J. Non-Newt. Fl. Mech*, 69 (1997) 195-206.
- [19] P. D. Olmsted, O. Radulescu, and C.-Y. D. Lu, The Johnson-Segalman model with a diffusion term in Couette flow, *J. Rheol*, (in press, 1999).
- [20] T. C. B. McLeish, Stability of the interface between 2 dynamic phases in capillary-flow of linear polymer melts, *J. Poly. Sci. B-Poly. Phys.*, 25 (1987) 2253-2264.
- [21] C.-Y. D. Lu, P. D. Olmsted, and R. C. Ball, The effect of non-local stress on the determination of shear banding flow, *Phys. Rev. Lett.*, (submitted, 1999).
- [22] O. Radulescu, P. D. Olmsted, and C.-Y. D. Lu, Shear banding in reaction-diffusion models, *Rheol. Acta* (in press, 1999).
- [23] A. W. El-Kareh and L. G. Leal, Existence of solutions for all Deborah numbers for a non-newtonian model modified to include diffusion, *J. Non-Newt. Fl. Mech.*, 33 (1989) 257-287.
- [24] P. Brunovský and D. Ševčovič, Explanation of spurt for a non-Newtonian fluid by a diffusion term, *Quart. J. Appl. Math.*, 3 (1994) 401-426.

- [25] N. A. Spenley, X. F. Yuan, and M. E. Cates, Nonmonotonic constitutive laws and the formation of shear-banded flows, *J. Phys. II (France)*, 6 (1996) 551-571.
- [26] J. R. A. Pearson, Flow curves with a maximum, *J. Rheol.*, 38 (1994) 309-331.
- [27] P. D. Olmsted and P. M. Goldbart, Isotropic-nematic transition in shear flow: State selection, coexistence, phase transitions, and critical behavior, *Phys. Rev.*, A46 (1992) 4966-4993.
- [28] P. D. Olmsted and C.-Y. D. Lu, Coexistence and phase separation in sheared complex fluids, *Phys. Rev.*, E56 (1997) 55-58.
- [29] R. W. Mair and P. T. Callaghan, Shear flow of wormlike micelles in pipe and cylindrical couette geometries as studied by nuclear magnetic resonance microscopy, *J. Rheol.*, 41 (1997) 901-924.
- [30] M. M. Britton and P. T. Callaghan, Two-phase shear band structures at uniform stress, *Phys. Rev. Lett.*, 78 (1997) 4930-4933.
- [31] J. P. Decruppe, E. Cappelaere, and R. Cressely, Optical and rheological properties of a semi-diluted equimolar solution of cetyltrimethylammonium bromide and potassium bromide, *J. Phys. II (France)*, 7 (1997) 257-270.
- [32] S. Lerouge, J. P. Decruppe, and C. Humbert, Shear banding in a micellar solution under transient flow, *Phys. Rev. Lett.*, 81 (1998) 5457-5460.
- [33] R. J. Gordon and W. R. Schowalter, *Trans. Soc. Rheol.*, 16 (1972) 79.
- [34] P. A. Lagerstrom, *Matched Asymptotic Expansions: ideas and techniques* (Springer-Verlag, New York, 1988).
- [35] M. Bode, Front-bifurcations in reaction-diffusion systems with inhomogeneous parameter distributions, *Physica*, D106 (1997) 271-286.
- [36] Examples (from biology and solid-state physics) of non-potential reaction-diffusion systems for which the dominance principle does not apply are described in Ref. [35]. In these special systems propagation of the interface is possible in both directions, depending on the shape of the interface profile.
- [37] M. Renardy and Y. Renardy, Derivation of amplitude equations and analysis of side band instabilities in two-layer fluids, *Phys. Fluids*, A7 (1993) 2738-2762.
- [38] B. Khomani and H. K. Ganpule, An investigation of interfacial instabilities in the superposed channel flow of viscoelastic fluids, *J Non-Newt. Fl. Mech.*, 81 (1999) 27-69.
- [39] X.-F. Yuan, Dynamics of mechanical interface in shear-banded flow, *Europhys. Lett.*, 46 (1999) 542-548.
- [40] J. L. Goveas and G. H. Fredrickson, Curvature-driven shear-banding in polymer melts, *J. Rheol.*, (in press, 1999).